The Astronomical Journal, 124:2749–2755, 2002 November

ABUNDANCES OF MOLECULAR SPECIES IN BARNARD 68

James Di Francesco,[1] Michiel R. Hogerheijde,[2] and William J. Welch
Radio Astronomy Laboratory, 601 Campbell Hall, University of California, Berkeley, Berkeley, CA 94705-3411;
james.difrancesco@nrc.ca

and

Edwin A. Bergin
Harvard-Smithsonian Center for Astrophysics, 60 Garden Street, MS 42, Cambridge, MA 02138
Received 2002 June 14; accepted 2002 August 6

ABSTRACT

Abundances for five molecules ($C^{18}O$, CS, NH_3, H_2CO, and C_3H_2) and one molecular ion (N_2H^+) and upper limits for the abundances of one molecule (^{13}CO) and one molecular ion (HCO^+) are derived for gas within the Bok globule Barnard 68 (B68). The abundances were determined using our own BIMA millimeter interferometer data and single-dish data gathered from the literature, in conjunction with a Monte Carlo radiative transfer model. Since B68 is the only starless core to have its density structure strongly constrained via extinction mapping, a major uncertainty has been removed from these determinations. All abundances for B68 are lower than those derived for translucent and cold dense clouds, but perhaps significantly only for N_2H^+, NH_3, and C_3H_2. Depletion of CS toward the extinction peak of B68 is hinted at by the large offset between the extinction peak and the position of maximum CS line brightness. Abundances derived here for $C^{18}O$ and N_2H^+ are consistent with other, recently determined values at positions observed in common.

Key words: ISM: abundances — ISM: globules — ISM: individual (Barnard 68) — ISM: molecules — stars: formation

1. INTRODUCTION

Stars form out of cores of dense molecular gas. Such cores can be embedded deeply within molecular clouds, but numerous examples of isolated cores, e.g., Bok globules (Bok & Reilly 1947; Clemens & Barvainis 1988), have also been identified as dark patches of high visual extinction against rich stellar backgrounds. As isolated cores, Bok globules can be relatively free from the influences of nearby star-forming events and so can provide very simple and pristine examples of the physical and chemical structures of cores prior to the formation of low-mass stars. In this paper, we examine the abundances of several species of molecules or molecular ions in the globule Barnard 68 (B68; Barnard 1919).

B68 (also known as CB 82 or LDN 57) is an Ophiuchus dark cloud, located at ~125 pc (de Geus, de Zeeuw, & Lub 1989),[3] within the Loop I superbubble. Figure 1 shows an *R*-band image of B68 obtained from the CDS/Aladin sky atlas, revealing its compact, roundish morphology. B68 has no evidence of star formation within its interior, e.g., from detections of outflow wings in lines of ^{12}CO (Avery et al. 1987) or from an *IRAS* point source (Parker 1988).[4] Furthermore, continuum emission at $\lambda = 1.3$ mm toward B68 has not been detected (Reipurth, Nyman, & Chini 1996; Launhardt & Henning 1997).

B68 is unique in that it is the only starless Bok globule to have its density structure well defined. Using the extinction of the background Galactic bulge K giant population, Alves, Lada, & Lada (2001, hereafter ALL01) found an azimuthally averaged radial column density profile for B68 that was well matched with that of an isothermal, self-gravitating Bonnor-Ebert sphere, specifically, one with a near-critical center-to-edge density contrast of 16.5 (Bonnor 1956; Ebert 1955). The robust definition of density within B68 removes a major uncertainty toward determining its molecular abundances. Recently, Bergin et al. (2002) used single-dish maps of B68 in conjunction with models specifically incorporating the ALL01 Bonnor-Ebert density structure to ascertain radial variations in $C^{18}O$ and N_2H^+ abundance, with the lowest values occurring at the highest extinctions within B68. Hotzel et al. (2002) also found evidence for depletion of CO isotopes with extinction from their own single-dish maps and a reanalysis of the ALL01 data. Each group speculated that these molecules sublimate from the gas phase onto dust grains at the high densities and low temperatures in the B68 interior. A similar interpretation was made by Tafalla et al. (2002) to explain the radial depletion of CS and $C^{18}O$ in the interiors of five other starless cores, although N_2H^+ was not depleted and NH_3 was enhanced at these locations.

We explore further the abundances of several molecules or molecular ions within B68, incorporating the ALL01 Bonnor-Ebert density structure into our own models. New observations of B68 made with the Berkeley-Illinois-Maryland Association (BIMA) millimeter array are used to obtain upper limits on abundances of ^{13}CO and HCO^+ near the extinction peak found by ALL01, i.e., at R.A. = $17^h22^m38^s.6$, decl. = $-23°49'46''.0$ (J2000). Upper limits to $C^{18}O$ and N_2H^+ abundances are also derived at this

[1] Currently at Herzberg Institute of Astrophysics, National Research Council of Canada, 5071 West Saanich Road, Victoria, BC V9E 2E7, Canada.

[2] Currently at Steward Observatory, University of Arizona, 933 North Cherry Avenue, Tucson, AZ 85721-0065.

[3] A distance range of 60–205 pc for the Ophiuchus dark clouds was formally estimated by de Geus et al., with their center defined as 125 ± 25 pc.

[4] The $24'' \times 5''$ (P.A. of 94°) error ellipse of the *IRAS* point source 17194−2351, associated with B68 by Clemens & Barvainis, is centered ~3′ beyond the opaque edge of B68 seen in Fig. 1.

position and are consistent with values derived by Bergin et al. In addition, single-dish detections of lines reported in the literature are used to derive abundance values for $C^{18}O$, CS, N_2H^+, NH_3, H_2CO, and C_3H_2 toward positions in B68 offset from the extinction peak. We describe the BIMA observations and single-dish data in § 2 and our method of determining abundances with a Monte Carlo radiative transfer code in § 3. The derived results are discussed in § 4. A concluding summary is found in § 5.

2. OBSERVATIONS AND RESULTS

2.1. *BIMA Observations*

Figure 1 shows the position of the one pointing made toward B68 with the BIMA millimeter interferometer at Hat Creek, California, i.e., at R.A. = $17^h22^m38^s.6$, decl. = $-23°49'42''.0$ (J2000), approximately 4″ north of the extinction peak. Both ^{13}CO 1–0 and $C^{18}O$ 1–0 were observed simultaneously during tracks on 2001 May 9 and May 20, and N_2H^+ 1–0, HCO^+ 1–0, and HOC^+ 1–0 were observed simultaneously on 2001 April 24 and May 14. Figure 1 also shows the minimum and maximum FWHM sizes of the BIMA primary beams at the frequencies of ^{13}CO 1–0 and HCO^+ 1–0. Each line was observed in its own correlator window of 6.25 MHz width, with each window set to have 512 channels of 12.2 kHz width (i.e., ~0.03 km s^{-1} at 110 GHz). The correlators were tuned so the central channel of each window corresponded to a V_{LSR} of +3.4 km s^{-1}, the velocity centroid of $C^{18}O$ 2–1 found by Wang et al. (1995).

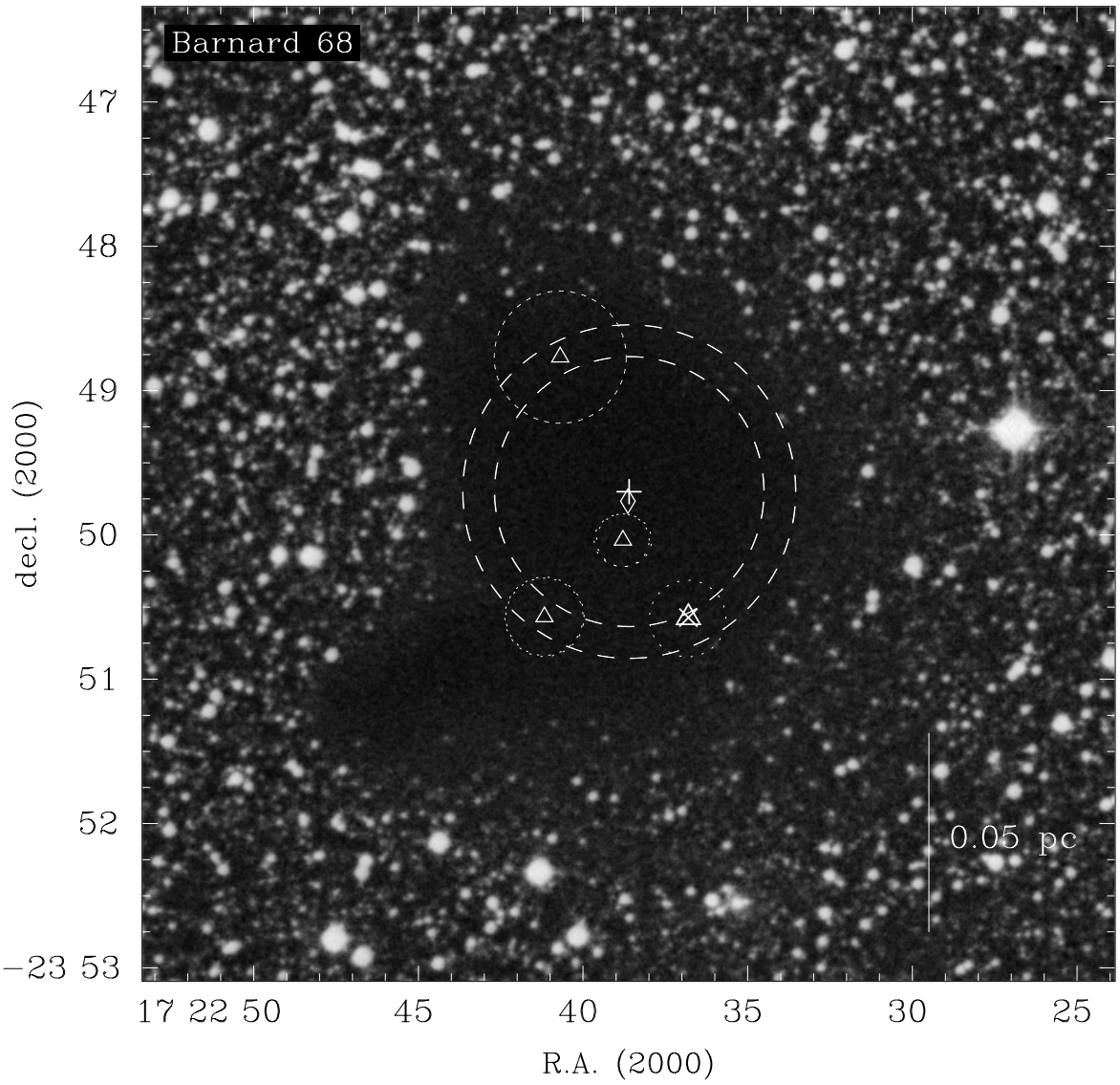

FIG. 1.—ESO MAMA *R*-band image of B68 (from CDS/Aladin). The position of maximum visual extinction determined by ALL01, i.e., the extinction peak, is denoted by a diamond. The central pointing position of the BIMA observations is shown as a plus sign, and the FWHMs of the BIMA primary beams at 89.2 GHz (HCO^+ 1–0) and 110.2 GHz (^{13}CO 1–0) are shown, respectively, as the outer and inner dashed circles. The positions and FWHM beam sizes of single-dish line observations from the literature are shown, respectively, as triangles and dotted circles. From north to south, these positions are from Launhardt et al. (1998; CS 2–1), Benson et al. (1998; N_2H^+ 1–0 and C_3H_2 2_{12}–1_{01}), Wang et al. (1995; $C^{18}O$ 2–1 and H_2CO 3_{21}–2_{11}), and Lemme et al. [1996; NH_3 (1, 1)]. The cross denotes the position of B68 from Clemens & Barvainis (1988). The error ellipse of the nearby far-infrared point source IRAS 17194−2351 is located south of B68 off the side of the image shown. The scale bar size assumes a distance to B68 of 125 pc.

TABLE 1
SUMMARY OF LINE OBSERVATIONS OF B68

Line	Observatory[a]	Beam FWHM[b] (arcsec × arcsec)	Extinction Peak Offset[c] (arcsec)	Reference
^{13}CO 1–0	BIMA	17.1 × 4.7	4.03	1
C^{18}O 1–0	BIMA	17.7 × 4.5	4.03	1
C^{18}O 2–1	CSO	30 × 30	59.3[d]	2
CS 2–1	FCRAO	46 × 46	66.2[d]	3
HCO$^+$ 1–0	BIMA	18.5 × 7.0	4.03	1
HOC$^+$ 1–0	BIMA	18.9 × 7.0	4.03	1
N_2H^+ 1–0	BIMA	17.7 × 6.6	4.03	1
N_2H^+ 1–0	Haystack	18 × 18	16.3	4
NH_3 (1, 1)	Effelsberg	40 × 40	54.5	5
H_2CO 3_{12}–2_{11}	CSO	30 × 30	59.3	2
C_3H_2 2_{12}–1_{01}	Haystack	18 × 18	16.3	4

[a] BIMA: Berkeley-Illinois-Maryland Array; CSO: Caltech Submillimeter Observatory; FCRAO: Five College Radio Astronomy Observatory.
[b] Synthesized beam FWHM for BIMA data, observed beam FWHM for single-dish data reported by authors.
[c] Offset of data from the extinction peak.
[d] Position of peak emission from map, where line characteristics were reported by authors.
REFERENCES.—(1) This work. (2) Wang et al. 1995. (3) Launhardt et al. 1998. (4) Benson, Caselli, & Myers 1998. (5) Lemme et al. 1996.

Each track was only 4–5 hr in duration given the low maximum elevation of B68 from Hat Creek (i.e., $\sim$25°). Visibility phases were calibrated by observing 1733−130 for 5 minutes approximately every 30 minutes over 800 MHz bandwidth in the lower or upper sideband. Visibility amplitudes were calibrated by similarly observing Uranus for 8 minutes at the end of each track. All data were reduced using standard routines within the MIRIAD software package (Sault, Teuben, & Wright 1995). All channels were cleaned to 2 σ rms intensity levels.

Line emission was not detected at any of the frequencies observed, at any positions toward B68 within the $\sim$2′ FWHMs of the BIMA primary beams. Binning together several channels or tapering the data with variously sized Gaussians did not change this result. Table 1 summarizes these data, listing the lines, the source observatory, the synthesized beam FWHMs, and the angular offset of the BIMA pointing from the extinction peak. The 1 σ rms sensitivities attained per channel ranged from 1.0 K for HOC$^+$ 1–0 to 1.5 K for ^{13}CO 1–0 and were measured by sampling all channels within a 40″ × 40″ box centered at the pointing center. Upper limits (at 3 σ) to the integrated intensities of these lines ranged from 0.21 to 0.34 Jy beam^{-1} km s^{-1} (or 0.25–0.44 K km s^{-1}) assuming a line width equal to 0.4 km s^{-1}, the typical FWHM of optically thin lines in B68 found by Wang et al.

2.2. *Single-Dish Observations*

We surveyed the literature to find previous detections of molecular line emission toward B68 from which abundances could be measured. Fortunately, B68 was included in numerous surveys of dark globules for molecular line emission. Early detections of lines include those of ^{12}CO 1–0 and ^{13}CO 1–0 by Martin & Barrett (1978) and Leung, Kutner, & Mead (1982), ^{12}CO 2–1 by Avery et al. (1987) and Clemens, Yun, & Heyer (1991), and ^{12}CO 3–2 by Avery et al. Furthermore, NH_3 (1, 1) and (2, 2) were detected by Martin & Barrett and Bourke et al. (1995). Although these data certainly indicate that line emission is associated with B68, we exclude them from analysis because of their relatively low angular resolution, i.e., more than 60″ FWHM.

More recent detections of line emission from various species toward B68 have been made with resolutions of less than 60″ FWHM, including those of C^{18}O 2–1 and H_2CO 3_{12}–2_{11} by Wang et al., CS 2–1 by Launhardt et al. (1998), N_2H^+ 1–0 and C_3H_2 2_{02}–1_{01} by Benson, Caselli, & Myers (1998), and NH_3 (1, 1) by Lemme et al. (1996). Other recent detections include those of C^{18}O 1–0 and N_2H^+ 1–0 by Bergin et al. and ^{13}CO 1–0, C^{18}O 1–0 and 2–1 by Hotzel et al., but we exclude those data from our analysis because abundances have been specifically determined from them by the respective authors. An interesting nondetection in the literature is that of SO 1_0–0_1 by Codella & Muders (1997), but their map was centered on the nearby *IRAS* point source and did not overlap the region of extinction modeled by ALL01. The methods of observation and reduction relevant to these data are described in these references and are not reproduced here.

In the higher resolution single-dish studies, the positions where line characteristics were specifically reported vary widely. Figure 1 shows the positions and resolutions of observations from these studies against the *R*-band image of B68. Table 1 also lists the lines observed, the source observatories, the resolutions attained, and the angular offsets of the single-dish data from the extinction peak of the reported line characteristics. The positions listed in Table 1 for C^{18}O 2–1, CS 2–1, and N_2H^+ 1–0 are those of peak line intensity from their respective maps, where line characteristics were specifically reported. (H_2CO 3_{12}–2_{11} and C_3H_2 2_{02}–1_{01} were observed at only these positions by the respective authors.) It is interesting to note that these positions are not coincident with the extinction peak. The C^{18}O and CS positions are approximately coincident with an arc of maximal C^{18}O 1–0 integrated intensity centered at the extinction peak noted by

Bergin et al. (see their Fig. 1*a*), and the N_2H^+ position is approximately coincident with the "arc" of maximal N_2H^+ 1–0 integrated intensity around the extinction peak also noted by Bergin et al. (see their Fig. 1*b*).[5]

3. MONTE CARLO RADIATIVE TRANSFER MODELS

Molecular line data can place strong limits on molecular abundances within B68 because its density structure has been so well constrained by ALL01. For example, abundances can be estimated by using a Monte Carlo code to calculate the radiative transfer, molecular excitation, and line emission through a model of a dense core with a specific density profile, and varying abundances within the model until the output matches the observed data. For this purpose, we used the one-dimensional Monte Carlo code of Hogerheijde & van der Tak (2000), which can solve molecular excitation coupled with line and continuum radiative transfer in core models. This code is especially useful for application to B68. First, model fluxes can be found at positions arbitrarily offset from the central line of sight, to simulate observations of B68 at positions offset from the extinction peak. Second, the model fluxes can be sampled with the spatial frequency coverage of actual interferometer data to estimate how much emission may have been resolved out in those cases. Recently, van Zadelhoff et al. (2002) compared eight molecular excitation/radiative transfer codes, including that of Hogerheijde & van der Tak, and found that all codes give results to within 10% of one another, even at high opacity.

For models of B68, we assumed the thermal and density structure given by ALL01, i.e., an isothermal sphere with an outer radius of 12,500 AU and a "Bonnor-Ebert parameter" ξ_{max} of 6.9, corresponding to a center-to-edge density ratio of 16.5. Following ALL01, we assumed a temperature in our models of 16 K, as derived by Bourke et al. from NH_3 observations of B68. (An alternative temperature profile is considered in § 4.1 below.) The ξ_{max} parameter identifies the particular solution from the family that solves the second-order differential equation characterizing a Bonnor-Ebert sphere. We determined the density in 30 linearly spaced concentric shells by solving that differential equation with a fourth-order Runge-Kutta method (see Press et al. 1992). The central density in the ALL01 model for B68 is $\sim 2.5 \times 10^5$ cm^{-3}.

Molecular abundances were assumed to be constant with radius, although abundance gradients within B68 are quite possible for the molecular species considered here. For example, Bergin et al. found edge-to-center contrasts in the abundances of $C^{18}O$ and N_2H^+ to be 100 and 2, respectively, using their own maps of B68. With only single pointings for the single-dish data and nondetections for the interferometer data, we can derive abundance values or upper limits only at the positions listed in Table 1, averaged over the respective lines of sight and beamwidths, and cannot probe for abundance gradients. Gradients should not produce dramatic differences in the abundances we derive, however, given the small sizes of the beamwidths relative to the spatial extent of B68. For example, we note in § 4.2 little difference between our abundances of $C^{18}O$ and N_2H^+ and those derived by Bergin et al. at positions observed in common, despite our different abundance profiles.

The velocity field of the gas was assumed to have a turbulent line width of 0.4 km s^{-1} (see Wang et al.; since the lines are optically thin at the abundances found, the integrated intensity is independent of the adopted turbulent line width). We assume that each shell is stationary, although Bergin et al. suggest velocity variations within B68 may be significant. For reasons similar to those cited above for abundance gradients, we did not consider radial variations of line width.

In each shell, level populations were determined assuming standard collision rates for each molecule. The expected sky brightness distributions were then calculated using a $256 \times 256 \times 100$ cube with $1'' \times 1'' \times 0.04$ km s^{-1} elements. To compare models with interferometer data, "visibility" data sets were produced from the cubes using the MIRIAD task *uvmodel* and the antenna baselines from the original data. These latter data sets were inverted, cleaned, and restored in the same manner as the actual data and velocity-integrated line intensities calculated. By properly accounting for spatial filtering in this manner, we estimated BIMA would have recovered only ~20% of the flux emitted from an ALL01 Bonnor-Ebert sphere in B68. To compare models with single-dish data, the original cubes were convolved with Gaussians with widths appropriately representing the resolution of the respective observations. The abundances were varied until the observational data were well matched.

4. ABUNDANCES

Table 2 lists the fractional abundances of the sampled molecular species at various positions toward B68, constrained with the data described in § 2 and estimated by using the method described in § 3 (assuming models with the Bonnor-Ebert density profile of ALL01). The BIMA data yield the first upper limits to the abundances of HCO^+ toward the extinction peak of B68, as well as upper limits to the abundances of ^{13}CO, $C^{18}O$, and N_2H^+ at the same location. Since collision rates are not available for HOC^+, we do not attempt to place limits on its abundance. In addition, single-dish data of B68 from the literature yield abundance values of H_2CO, CS, NH_3, and C_3H_2 toward B68 for the first time, but at various positions offset from the extinction peak. Finally, other single-dish data of B68 from the literature yield new abundance values of $C^{18}O$ and N_2H^+ at some of these latter locations.

4.1. *Comparison with Other Clouds*

How do the abundances derived for B68 here compare to those derived for other clouds? "Standard" cloud molecular abundances with which to base comparisons are difficult to define given wide variations in chemical environment or evolutionary epoch in the interstellar medium. To provide some comparison, Table 2 also lists the fractional abundance estimates of the same species in clouds similar in character to B68, obtained directly from the literature but made without the detailed foreknowledge of cloud density structure now available for B68. The first set, for "translucent clouds," are those listed by Turner (2000) for small, round Clemens & Barvainis clouds with edge-to-center

[5] An N_2H^+ 1–0 map toward B68 recently made by Caselli et al. (2002) confirms that this position is that of peak intensity, although their data are not Nyquist sampled and are of lower resolution than those of Benson et al. and Bergin et al.

TABLE 2
ABUNDANCES OF VARIOUS MOLECULAR CLOUDS

Species	B68[a]	Translucent Clouds[b]	TMC-1[c]	L134N[c]
^{13}CO	<1.3(−7)	...	8.9(−7)[d]	8.9(−7)[d]
$C^{18}O$	<1.3(−7)	...	1.6(−7)[d]	1.6(−7)[d]
$C^{18}O$	3.0(−8)	...	1.6(−7)	1.6(−7)
CS 2–1.....	4.0(−10)	1.1(−9)	1(−8)	1(−9)
HCO^+.....	<1.4(−10)	2(−9)	8(−9)	8(−9)
HOC^+.....	...	...	...	...
N_2H^+	<1.3(−10)	1(−9)	5(−10)	5(−10)
N_2H^+	2.0(−11)	1(−9)	5(−10)	5(−10)
NH_3	7.0(−10)	2.1(−8)	2(−8)	2(−7)
H_2CO.....	4.0(−10)	6.3(−9)	2(−8)	2(−8)
C_3H_2	1.2(−11)	3.6(−8)	3(−8)	2(−9)

NOTE.—$a(-b)$ denotes $a \times 10^{-b}$.

[a] Abundances are derived at the positions listed in Table 1 assuming a Bonnor-Ebert model of ALL01 and $T = 16$ K. Upper limits are derived from interferometer nondetections, while values are derived from the single-dish detections described in the literature. Using the temperature profile suggested by Zucconi, Walmsley, & Galli (2001) increases abundances by factors of 2–3.

[b] Translucent cloud abundances from Turner (2000) are defined for a fiducial cloud of constant abundance with edge-to-center visual extinction of 2.0. The values listed are averages from hydrostatic equilibrium polytropic models and constant-density models.

[c] Cold dense cloud abundances are from Ohishi, Irvine, & Kaifu (1992), assuming $N(H_2) = 10^{22}$ cm^{-2}.

[d] Derived from ^{12}CO abundance assuming $^{12}C/^{13}C = 90$ or $^{16}O/^{18}O = 500$.

visual extinctions of 2.0. These clouds were modeled with constant abundance, and the listed values are averages between the results of a hydrostatic equilibrium polytropic model and an $n(r) \propto r^0$ model.[6] The second set, for "cold dense clouds," are those compiled by Ohishi, Irvine, & Kaifu (1992) for a single position in TMC-1 or L134N and were made using column density estimates from many authors, assuming $N(H_2) = 10^{22}$ cm^{-2} (see Turner 2000, Pratap et al. 1997, or Dickens et al. 2000 for alternative estimates). The abundances from Turner and Ohishi et al. in Table 2 should not be regarded as universal. For example, Turner notes that abundances can vary by an order of magnitude both between different translucent clouds and within larger, dense clouds (presumably determined using similar assumptions).

Table 2 shows that every value of molecular abundance we derive for B68 is less than the lowest value derived for other clouds. From the BIMA data, we find the upper limits to the ^{13}CO, HCO^+, and N_2H^+ abundances in B68 are lower than values derived for other clouds by factors of 7, 14, and 4 respectively. (The upper limit to the $C^{18}O$ abundance is similar to the lowest value found for other clouds.) From the various single-dish data, we find the $C^{18}O$, CS, and H_2CO abundances differ least, by roughly an order of magnitude or less, with the B68 abundances lower than the lowest values derived for other clouds by factors of only 5, 3, and 16, respectively, at the locations observed. However, the N_2H^+, NH_3, and C_3H_2 abundances differ the most, by over an order of magnitude, with those of B68 lower by factors of 25, 29, and 170, respectively, at the locations observed.

The assumption in our models of an isothermal Bonnor-Ebert sphere, at the same 16 K temperature derived by Bourke et al. and used by ALL01, has likely minimized the resulting abundance values we obtain. Other temperature profiles, such as those suggested for Bonnor-Ebert spheres by Zucconi, Walmsley, & Galli (2001; see also Evans et al. 2001) that have cooler temperatures at small radii, may be more appropriate. For example, Bergin et al. assumed for their models of B68 the Zucconi et al. radial temperature profile with a global reduction of 2 K, in addition to the ALL01 density profile. With this same temperature profile in our models, the values in Table 2 increase by factors of only 2–3. Therefore, using this radial temperature profile would bring the abundances of $C^{18}O$, CS, and H_2CO at the positions observed in B68 even more in line with the abundances found for other cloud types. However, the abundances of N_2H^+, NH_3, and C_3H_2 at other positions would still remain lower than those of other clouds by an order of magnitude or more.

Only N_2H^+, NH_3, and C_3H_2 are arguably depleted in B68, given the values shown in Table 2 and assuming a typical order of magnitude abundance variation between and within similar clouds. However, other species considered here still may be depleted in B68. Note that the degree to which the abundance of a particular species in B68 is low compared to those of other clouds appears related to the position across B68 that the respective data were obtained. The $C^{18}O$, CS, and N_2H^+ data from the literature were those of maximum line brightness from maps of B68, and H_2CO and C_3H_2 data were obtained only subsequently by the respective authors at those positions. (NH_3 was observed only at the Clemens & Barvainis position of B68.) Figure 1 and Table 2 together reveal that the less discrepant abundances are found at positions relatively far from the extinction peak but the more discrepant abundances are found at positions closer to the extinction peak (except

[6] According to B. E. Turner (2002, private communication), these two models produce results that differ at most by a factor of 1.35 for species that are highly dependent on density.

notably NH_3). This pattern suggests that C_3H_2 may be also depleted by some process related to extinction, e.g., the sublimation of gas-phase molecules onto grains, as suggested by Bergin et al. for $C^{18}O$ and N_2H^+ and Hotzel et al. for ^{13}CO and $C^{18}O$. This same idea may also explain how CS and H_2CO appear relatively undepleted in the outer, less extincted radii of B68. Moreover, the lack of bright emission in CS near the extinction peak hint that it may be also depleted at high extinction in B68. These speculations can be confirmed only after analyzing fully sampled, high-resolution line maps of B68.

4.2. *Comparison with Previous Abundance Determinations*

How do the abundances we derive compare with those found previously for B68? Bergin et al. found the $C^{18}O$ abundance in B68 rises from very low values at $A_V \ll 1$ to a peak of 1×10^{-7} at $A_V = 2$, and decreases to 1×10^{-9} at $A_V > 20$, a contrast of $\sim$100. In addition, Bergin et al. found the N_2H^+ abundance rises from very low values at $A_V \ll 1$ to a peak of 6×10^{-11} at $A_V = 3$, and decreases to 3×10^{-11} at $A_V > 20$, a contrast of $\sim$2. Any evidence of N_2H^+ depletion is remarkable, given its oft-described utility as a nondepleting probe of dense core interiors (e.g., see Tafalla et al. 2002).

Our interferometer data of $C^{18}O$ and N_2H^+ do not provide much additional support for the abundance model for B68 of Bergin et al. Our derived upper limits for $C^{18}O$ and N_2H^+ from the BIMA data are not particularly low, but they remain consistent with the still lower values found by Bergin et al. throughout the core. Also, the nondetection of compact line emission with BIMA suggests the low abundances found by Bergin et al. are not due to the single-dish beam dilution of small clumps of relatively abundant material. A spatially smoother model of gas density is indeed more appropriate for B68, such as the Bonnor-Ebert sphere suggested by the dust extinction maps.

The single-dish $C^{18}O$ and N_2H^+ data from the literature pertain only to one line of sight per transition toward B68, but provide strong support for the abundances derived by Bergin et al., if the same modified Zucconi et al. temperature profile is assumed. With this assumption, the $C^{18}O$ literature data, from a position offset from the extinction peak by 59″.4, yield an apparent abundance of $(6–9) \times 10^{-8}$, quite consistent with the $(3–9) \times 10^{-8}$ abundance range expected along this line of sight from the model of Bergin et al. Also, the N_2H^+ literature data, from a position offset from the extinction peak by 16″.3, yield an apparent value of $(4–6) \times 10^{-11}$, slightly larger than but still consistent with the $(3–4) \times 10^{-11}$ abundance range expected along this line of sight from the model of Bergin et al. Furthermore, the observed integrated intensities of these literature data at each respective location and our BIMA observations can be reproduced to within only a few percent with our own Monte Carlo models, assuming the ALL01 density profile, the modified Zucconi et al. temperature profile, and the Bergin et al. radial abundance profiles. (Note that here we relaxed the earlier assumption of constant abundance with radius.)

5. SUMMARY AND CONCLUSIONS

Using our own interferometer line data and single-dish line data culled from the literature of the Bok globule B68 and a Monte Carlo radiative transfer code, we derive abundances for $C^{18}O$, CS, N_2H^+, NH_3, H_2CO, and C_3H_2 and upper limits for abundances of ^{13}CO and HCO^+. Foreknowledge of the Bonnor-Ebert density configuration of B68, as found from extinction mapping by ALL01, has removed a major uncertainty that affected previous estimations of abundances in other clouds. We find molecular abundances in B68 are lower than those estimated previously for clouds similar to B68. The abundances of N_2H^+, NH_3, and C_3H_2 are lower than the lowest values determined for other clouds by 1.4, 1.5, and 2.2 orders of magnitude, respectively, but the abundances of the other species are lower only by 1 order of magnitude or less. Depletion of CS is suggested by the large offset between the position of maximum CS line brightness and the extinction peak. Furthermore, abundances of $C^{18}O$ and N_2H^+ derived using data from the literature at locations where line characteristics were reported are consistent with those derived by Bergin et al.

As shown by Bergin et al., fully sampled maps from single-dish telescopes can more effectively determine abundances within B68. Further maps of B68 can now be easily obtained using the new multibeam focal plane arrays on current single-dish telescopes. Furthermore, the upcoming generation of millimeter interferometers will have the sensitivity to provide additional data for combined maps of even higher resolution. With these data, more accurate molecular abundances will be determined for B68. For example, it will be interesting to determine if abundances of CS, HCO^+, NH_3, H_2CO, and C_3H_2 also vary with extinction, like ^{13}CO, $C^{18}O$, or N_2H^+. Similar abundance determinations across other isolated dense cores may also be possible, provided their density structures can be similarly well defined.

We thank the referee, Barry Turner, for insightful comments that improved this paper. In addition, we thank Leo Blitz for allowing this project to be pursued with the BIMA millimeter array. J. D.'s research in Berkeley was supported by the Radio Astronomy Laboratory. M. R. H.'s research in Berkeley was supported by the Miller Institute for Basic Research in Science. We also thank Charles J. Lada, João Alves, Tracy Huard, and Jon Swift for their help. This research has made use of the SIMBAD database and Aladin, both operated by CDS, Strasbourg, France.

REFERENCES

Alves, J. F., Lada, C. J., & Lada, E. A. 2001, Nature, 409, 159 (ALL01)
Avery, L. W., White, G. J., Williams, I. P., & Cronin, N. 1987, ApJ, 312, 848
Barnard, E. E. 1919, ApJ, 49, 1
Benson, P. J., Caselli, P., & Myers, P. C. 1998, ApJ, 506, 743
Bergin, E. A., Alves, J., Huard, T., & Lada, C. J. 2002, ApJ, 570, L101
Bok, B., & Reilly, E. F. 1947, ApJ, 105, 255
Bonnor, W. B. 1956, MNRAS, 116, 351
Bourke, T. L., Hyland, A. R., Robinson, G., James, S. D., & Wright, C. M., 1995, MNRAS, 276, 1067
Caselli, P., Benson, P. J., Myers, P. C., & Tafalla, M. 2002, ApJ, 572, 238
Clemens, D. P., & Barvainis, R. 1988, ApJS, 68, 257
Clemens, D. P., Yun, J. L., & Heyer, M. H. 1991, ApJS, 75, 877
Codella, C., & Muders, D. 1997, MNRAS, 291, 337
de Geus, E. J., de Zeeuw, P. T., & Lub, J. 1989, A&A, 216, 44
Dickens, J. E., Irvine, W. M., Snell, R. L., Bergin, E. A., Schloerb, F. P., Pratap, P., & Miralles, M. P. 2000, ApJ, 542, 870
Ebert, R. 1955, Z. Astrophys., 37, 217
Evans, N. J., II, Rawlings, J. M. C., Shirley, Y. L., & Mundy, L. G. 2001, ApJ, 557, 193

Hogerheijde, M. R., & van der Tak, F. F. S. 2000, A&A, 362, 697
Hotzel, S., Harju, J., Juvela, M., Mattila, K., & Haikala, L. K. 2002, A&A, 391, 275
Launhardt, R., Evans, N. J., II, Wang, Y., Clemens, D. P., Henning, Th., & Yun, J. L. 1998, ApJS, 119, 59
Launhardt, R., & Henning, Th. 1997, A&A, 326, 329
Lemme, C., Wilson, T. L., Tieftrunk, A. R., & Henkel, C. 1996, A&A, 312, 585
Leung, C. M., Kutner, M. L., & Mead, K. N. 1982, ApJ, 262, 583
Martin, R. N., & Barrett, A. H. 1978, ApJS, 36, 1
Ohishi, M., Irvine, W. M., & Kaifu, N. 1992, in IAU Symp. 150, Astrochemistry of Cosmic Phenomena: Proceedings of the 150th Symposium of the International Astronomical Union, ed. P. D. Singh (Dordrecht: Reidel), 171
Parker, N. D. 1988, MNRAS, 235, 139
Pratap, P., Dickens, J. E., Snell, R. L., Miralles, M. P., Bergin, E. A., Irvine, W. M., & Schloerb, F. P. 1997, ApJ, 486, 862
Press, W. H., Teukolsky, S. A., Vetterling, W. T., & Flannery, B. P. 1992, Numerical Recipes (Cambridge: Cambridge Univ. Press)
Reipurth, B., Nyman, L.-Å., & Chini, R. 1996, A&A, 314, 258
Sault, R. J., Teuben, P. J., & Wright, M. C. H. 1995, in ASP Conf. Ser. 77, Astronomical Data Analysis Software and Systems IV, ed. R. A. Shaw, H. E. Payne, & J. J. E. Hayes (San Francisco: ASP), 433
Tafalla, M., Myers, P. C., Caselli, P., Walmsley, C. M., & Comito, C. 2002, ApJ, 569, 815
Turner, B. E. 2000, ApJ, 542, 837
van Zadelhoff, G.-J., Dullemond, C. P., van der Tak, F. F. S., Yates, J. A., Doty, S. D., Ossenkopf, V., Hogerheijde, M. R., Juvela, M., Wiesemeyer, H., & Schöier, F. L. 2002, A&A, in press
Wang, Y., Evans, N. J., II, Zhou, S., & Clemens, D. P. 1995, ApJ, 454, 217
Zucconi, A., Walmsley, C. M., & Galli, D. 2001, A&A, 376, 650